J Mater Sci (2007) 42:5020–5028
DOI 10.1007/s10853-006-0595-5

Vibration behavior of light metals: Al–Zn alloy and Mg–Al–Zn alloy

Fei-Yi Hung · Truan-Sheng Lui · Li-Hui Chen · Han-Wen Chang · Zong-Fu Chen

Received: 26 October 2005 / Accepted: 19 June 2006 / Published online: 23 February 2007

Abstract Both Al–Zn alloy and Mg–Al–Zn alloy are considered as high damping and light materials. This study investigated the effects of the structure and the composition on the vibration fracture characteristics of the Al–*x*Zn alloy and the Mg–*x*Al–Zn alloy under resonance. For Al–*x*Zn (x = 7, 11, 49, and 83 wt.%) alloys, under both constant force and initial-deflection conditions, the 7Zn specimen showed the greatest vibration life. For Mg–*x*Al–Zn (x = 3, 6, and 9 wt.%) alloys, experimental results indicate that the AZ31-F as-extruded samples showed a greater vibration life, while high Al fully annealed samples (AZ91-O) had greater vibration fracture resistance under constant force conditions.

Introduction

Owing to their capacity to reduce the overall weight, both aluminum alloys and magnesium alloys have been used extensively. Al–Zn alloys possess excellent working properties, damping capacity and mechanical properties. Also, one relevant study [1] has revealed that the damping capacity of Al–Zn alloy increases with increasing the Zn content, and attains a maximum value for damping capacity at 78 wt.% Zn. In addition, another relevant study [2–4] revealed that quenched specimens had better damping capacity than annealed specimens. From the above, it can be inferred that the vibration behavior of Al–*x*Zn alloy is related to its Zn content and cooling conditions. However, the vibration fracture characteristics of Al–Zn alloys have not yet been examined. The goal of this study is to investigate the vibration fracture behavior of quenched Al–*x*Zn alloys.

In addition, Magnesium alloys possess superior impact resistance and the electromagnetic interference characteristics [5–7], and have been used extensively in the auto industry and 3C (Computer, Communication and Consumer Electronic) products. Given that failure may occur due to vibration, the vibration fracture resistance should be taken into consideration in the design of Mg alloys. As of now, Mg–Al–Zn alloys are used extensively because of their excellent hardness, tensile properties and toughness [8–11]. Another aim of this study is to use as-extruded and annealed Mg–*x*Al–Zn (x = 3, 6, and 9 wt.%) alloys to investigate the effect of Al on the resonant vibration fracture behavior.

Experimental procedure

Master Al–*x*Zn alloys (x = 7, 11, 49, and 83 wt.%) were prepared and the alloy ingots were then solution treated at 350 °C for 24 h and extrusion was performed. The extrusive temperature for 7Zn, 11Zn, and 49Zn was 300 °C. About 320 °C was selected for the 83Zn specimen. Before performing the test, all specimens were given a heat-treatment at 370 °C for 1 h followed by water cooling to room temperature.

F.-Y. Hung (✉) · T.-S. Lui · L.-H. Chen · H.-W. Chang · Z.-F. Chen
Department of Materials Science and Engineering, National Cheng Kung University, Tainan 701, Taiwan, ROC
e-mail: fyhung@mail.mse.ncku.edu.tw

T.-S. Lui
e-mail: z7408020@email.ncku.edu.tw

For the commercial Mg–xAl–Zn extruded sheets, the AZ31-F, AZ61-F, and AZ91-F (F is defined as fabricated) specimens were selected for investigation. To avoid the effects of deformation twins and second-phase precipitate, the above three extruded specimens were given an annealing treatment. The annealing conditions for the AZ31-O and AZ61-O specimens were 355 °C for 6 h, while the AZ91-O specimen was held at 385 °C for 10 h, followed by water cooling to room temperature. The tensile mechanical properties at an initial strain rate of 7.5×10^{-4} s^{-1}, as well as the hardness of all the specimens, were ascertained. SEM and EDS were used for fracture analysis of the microstructures. In addition, a simple cantilever beam vibration system was used for the vibration experiments and damping measurements (see Fig. 1a), and the test specimens, Fig. 1b, which were rectangular with dimensions 100 mm × 15 mm × 2.5 mm, were fixed on end to the vibration shaker.

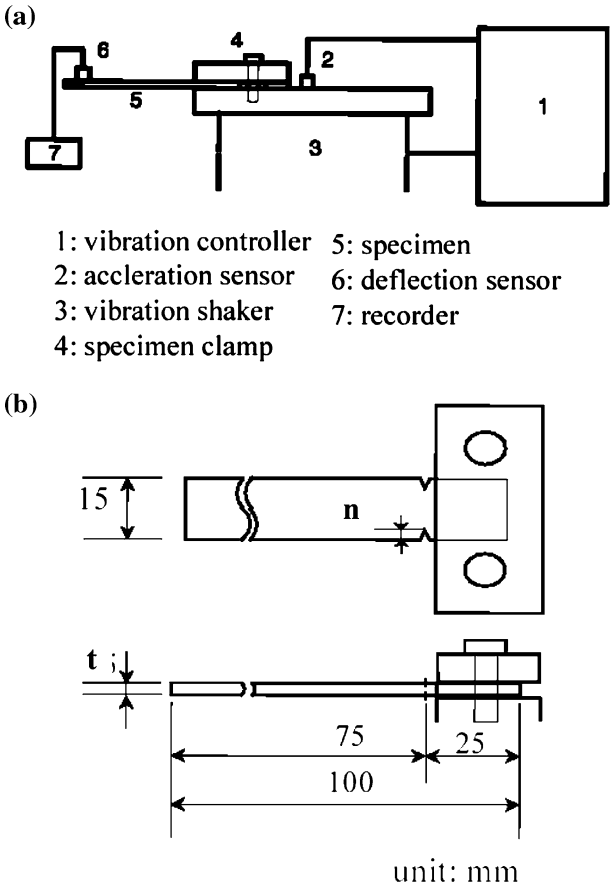

Fig. 1 (**a**) Schematic diagram of the vibration equipment and (**b**) shape and dimensions of the specimens for resonant vibration tests (t = 2.5 mm and n = 1.5 mm for Mg alloy, t = 3.0 mm and n = 1.0 mm for Al alloy)

Two circular notches near the clamp were made for observing microstructural evolution in the vicinity of the notch front. The vibration force was monitored using an acceleration sensor (vibration from top to bottom), and the deflection amplitude of the specimens at the end opposite the vibration shaker was measured using a deflection sensor. For the vibration frequency versus deflection amplitude curve, the maximum deflection amplitude is always at resonant frequency. The resonant frequency is taken as the frequency leading to the largest deflection and is determined by varying the vibration frequency continuously.

Results and discussion

Microstructure and vibration characteristics of Al–Zn alloys

Figure 2 shows the microstructures of the Al–xZn alloys after quenching. The equiaxed grains were found in the 7Zn, 11Zn, and 49Zn specimens. When increasing the Zn content up to 49 wt.%, the grain size of α-Al had a tendency to decrease. Notably, the 83Zn specimen possessed a lamellar structure composed of rich-Zn (() and rich-Al (). The tensile mechanical properties of the specimens are shown in Fig. 3. The results reveal that the 49Zn specimen showed superior values for hardness, yield strength (YS) and ultimate tensile strength (UTS), however, its ductility was lower than that of the other specimens. From observations of the tensile fractured characteristics (see Fig. 4), intergranular fractures were found in the 49Zn specimen, while the other specimens possessed dimple features. This shows that the brittleness effect was obviously active in the 49Zn specimen. It can be inferred that increasing the Zn content, thereby precipitate strengthening and decreasing the grain size, must be one reason why the strength was enhanced. When the Zn content was raised to 83 wt.%, the 83Zn structure was different from the structure of the other specimens. The strengthening mechanism of the lamellar structures ($\alpha + \beta$) was decided by the amount, solid solution content and interlamellar spacing of (phase and (phase. Relevant studies [12, 13] revealed that Zn-rich phase precipitated on the grain boundary and a G. P. zone formed on the grain in quenched Al–Zn alloys. This resulted in the occurrence of intergranular fractures and a reduction in ductility.

Figure 5 shows the D–N curves of the specimens under a fixed vibration force of 5 G (the resonant frequencies of the specimens were: 7Zn (54 ± 0.5 Hz), 11Zn (63 ± 0.5 Hz), 49Zn (64 ± 0.5 Hz), and 83Zn

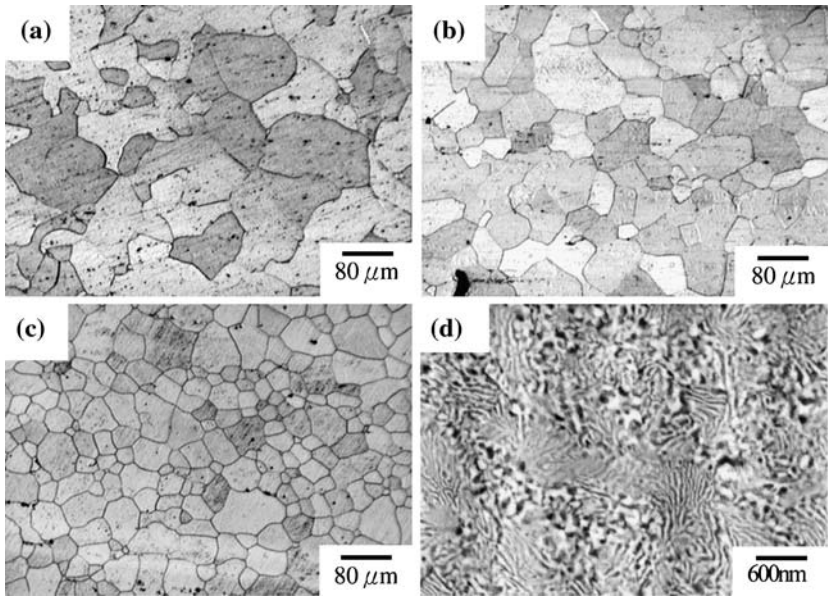

Fig. 2 Microstructure of the Al–*x*Zn alloys: (**a**) 7Zn, (**b**) 11Zn, (**c**) 49Zn, and (**d**) 83Zn

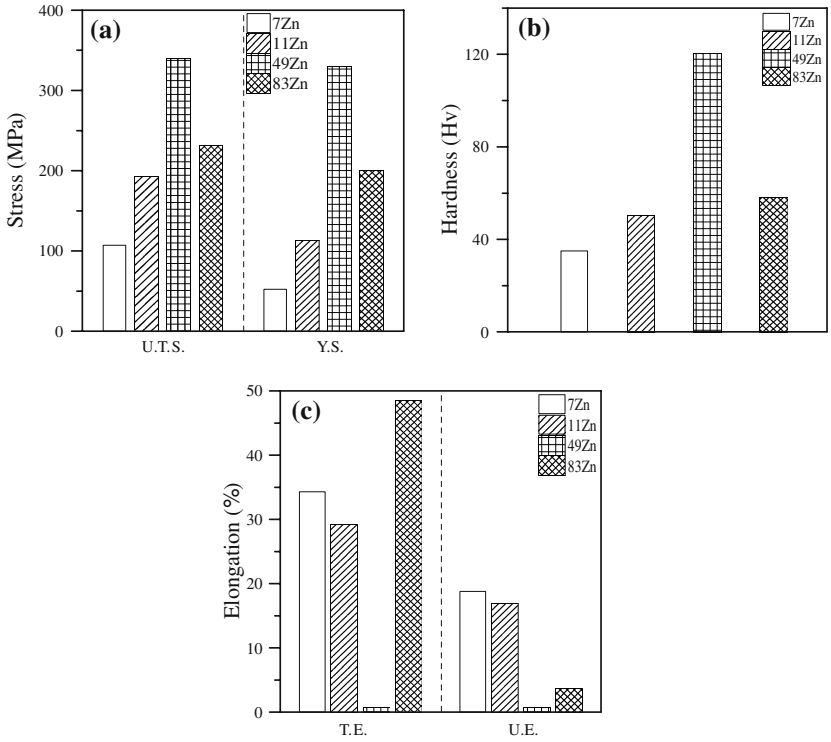

Fig. 3 Tensile mechanical properties of the specimens: (**a**) UTS and YS, (**b**) Hv, and (**c**) TE and UE

(62 ± 0.5 Hz)). The initial deflection amplitude of 49Zn was highest, followed by 11Zn, 7Zn, and 83Zn, respectively. This study avoided the effect of damping capacity by controlling the vibration force and measured the *D*–*N* curves of the specimens under constant initial deflection conditions. The initial deflection of the 49Zn specimen was 4.1 mm (see Fig. 5) and was selected as a standard for the other specimens. The vibration condition of the specimens under the initial deflection of 4.1 mm was: 7Zn (6 G, 54 ± 0.5 Hz), 11Zn (5.5 G, 63 ± 0.5 Hz), 49Zn (5 G, 64 ± 0.5 Hz) and 83Zn (7.3 G, 62 ± 0.5 Hz). Under constant initial deflection conditions, the vibration number for the 83Zn specimen was lowest, and the vibration number increased with decreasing the Zn content (see Fig. 6). Since the vibration fracture observations of Fig. 5 are similar to Fig. 6, this study uses Fig. 5 as an example for examination.

Figure 7 shows the vibration fractures of the specimens under a fixed vibration force of 5 G. The results reveal that the area fraction of the intergranular fractures

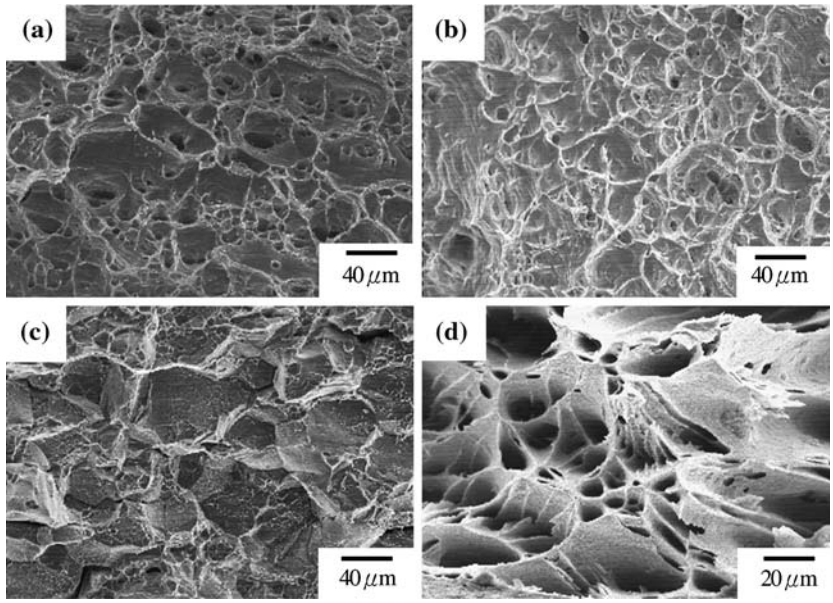

Fig. 4 Tensile fractured characteristics of the specimens: (**a**) 7Zn, (**b**) 11Zn, (**c**) 49Zn, and (**d**) 83Zn

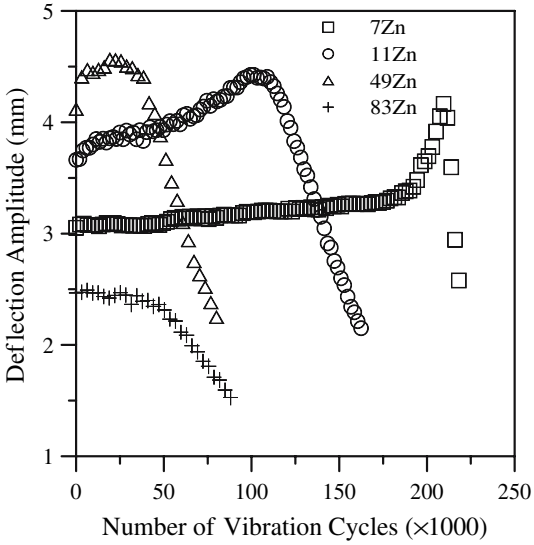

Fig. 5 *D–N* curves of the specimens under a fixed vibration force of 5 G

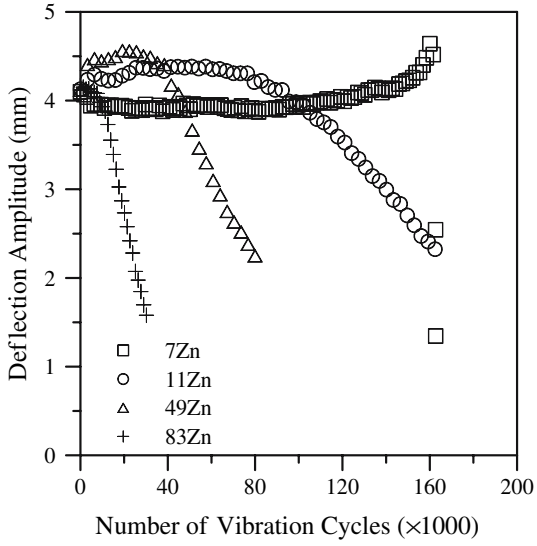

Fig. 6 *D–N* curves of the specimens under a fixed initial deflection amplitude of 4.1 mm

increases with increasing the Zn content until 49 wt.%. In addition, it can also be confirmed that intergranular fracture was induced by the precipitate on the grain boundary. As for the 83Zn specimen, no intergranular fracture behavior was observed (see Fig. 7d). Our observations and a relevant study [14] have verified that the slip bands decreased, grain size decreased, the precipitate grew and the G. P. zone increased with increasing the Zn content of Al–Zn alloy. The above resulted in variations in vibration fracture behavior. Increasing Zn content also makes it harder for the dislocations to move and causes the vibration life of specimens to deteriorate. In addition, according to relevant references [15] and the present data, it can be inferred that the internal friction of (((Al)/((Zn)) of the 83Zn specimen affected the damping capacity. Raising internal friction increases the vibration resistance of the material. From observations of crack propagation and the *D–N* curves, regardless of the vibration test conditions, the 7Zn specimen had the highest crack propagation resistance and the longest vibration life.

Resonant vibration characteristics of as-extruded Mg–Al–Zn alloys

The optical microstructures of as-extruded Mg–Al–Zn alloys are shown in Fig. 8. Owing to the hot-extrusion, deformed twins and signs of recrystallization can be

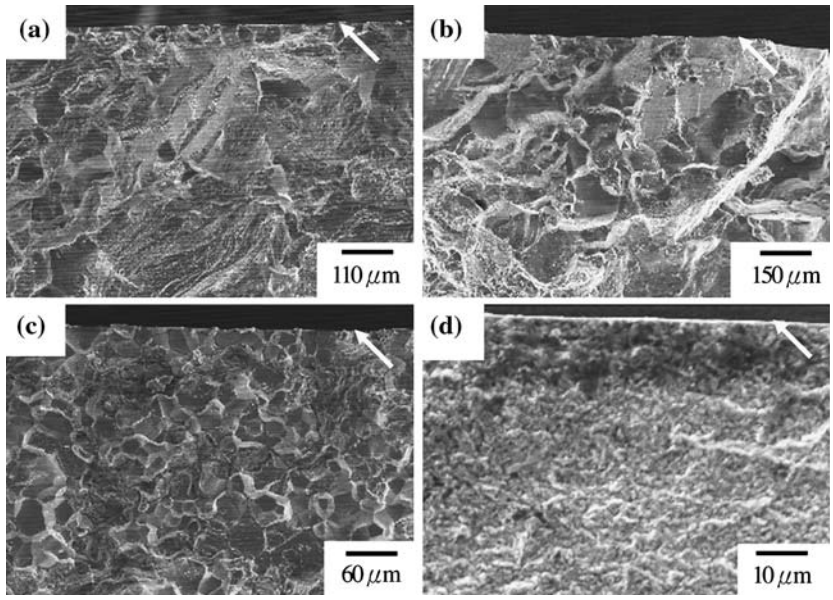

Fig. 7 Vibration fractures of the specimens under a fixed vibration force of 5 G (the *arrow* is upper surface): (**a**) 7Zn, (**b**) 11Zn, (**c**) 49Zn, and (**d**) 83Zn

found in the structures. The number of deformed twins in the grain decreases with increasing Al content. In addition, many particles were found in the grain boundaries of the F specimens. EDS analysis determined the composition of these particles (containing precipitate and proeutectic). The particle with Al content of ~44 wt.% is probably γ-$Mg_{17}Al_{12}$. For the AZ91-F specimen, no deformed twins were found in the grains, and a larger number of precipitates and proeutectic formed in the matrix. Owing to the hot-extrusion, a streamline shape of precipitate can be observed (see the arrow, Fig. 8b) and this is γ-$Mg_{17}Al_{12}$. These proeutectics were Al–Mn–Mg compounds. In addition, many Mg–Al–Zn compounds existed in the α-Mg matrix.

The microstructures of the annealed Mg–Al–Zn alloys are shown in Fig. 9. No twins were found in the AZ31-O or AZ61-O specimens, which shows that the precipitates re-dissolved into the α-Mg matrix. A similar phenomenon was observed in the AZ91-O specimens. Notably, a very small number of precipitates still existed in the AZ91-O matrix and they were Al–Mn–Mg compounds. Meanwhile, needle-like precipitates (see Fig. 9c) were also found in the AZ91-O structure. According to one study [16] and our own analysis, these precipitates are probably Mg–Al–Mn compounds. In addition, results show that the hardness of the O specimens was lower than that of the F specimens (see Fig. 10). The reason for this is that deformed twins and precipitates raise the hardness. As for the tensile deformation resistance, the tensile mechanical properties of both the F specimens and O specimens are shown in Fig. 11. Regardless of the structure, the

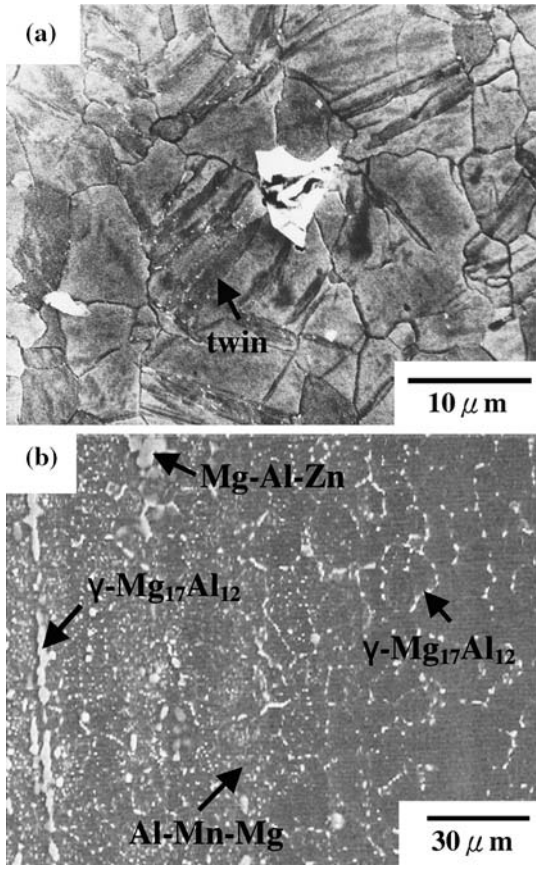

Fig. 8 Microstructure of the F alloys: (**a**) AZ31 and (**b**) AZ91

results reveal that each specimen had greater strength as the Al content was increased.

Figure 12 shows the *D*–*N* curves of the F specimens under a fixed vibration force of 1.3 G (the resonant

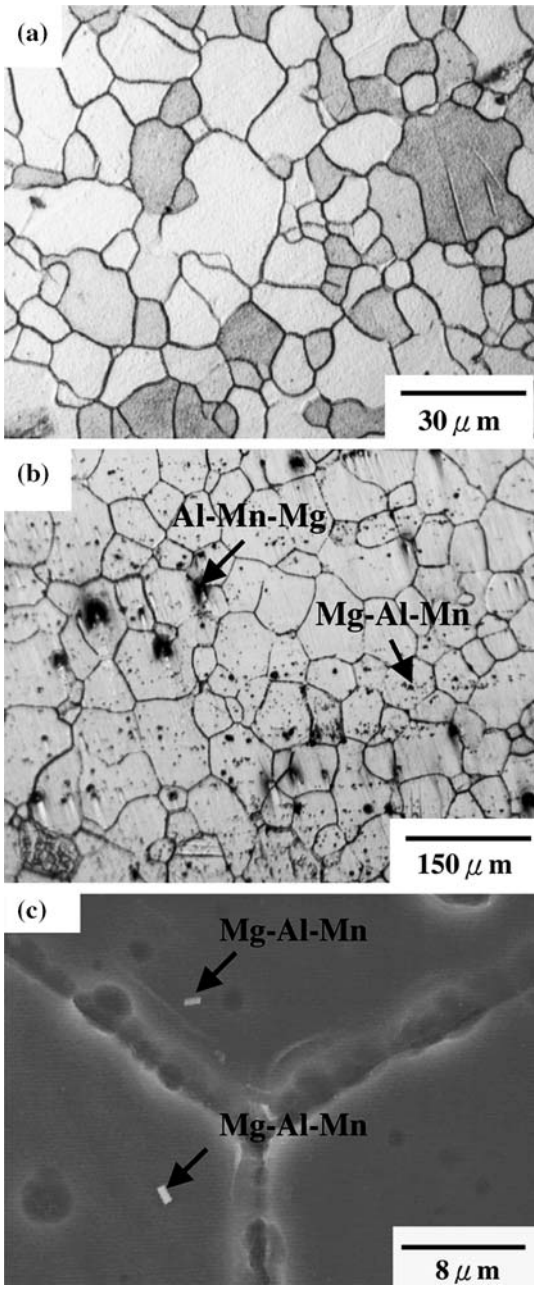

Fig. 9 Microstructure of the O alloys: (**a**) AZ31-O, (**b**)AZ91-O, and (**c**) AZ91-O

frequencies of the specimens have no change with variation of the composition, and the values are 36 ± 1 Hz). The vibration life can be known from conditions of constant force. So, constant initial deflection tests were not performed. Based on the data of Fig. 12, the vibration life in decreasing order was AZ31-F, AZ61-F, and then AZ91-F.

Figure 13 shows the vibration fractures of the AZ31-F specimens under a fixed vibration force of 1.3 G. The vibration cracks go through the original twins (see

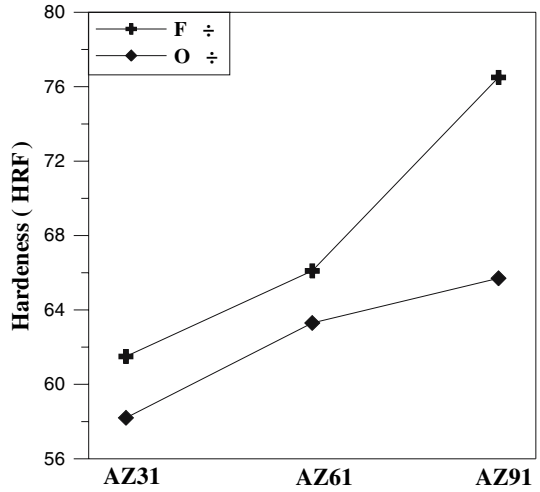

Fig. 10 Hardness of the F specimens and the O specimens

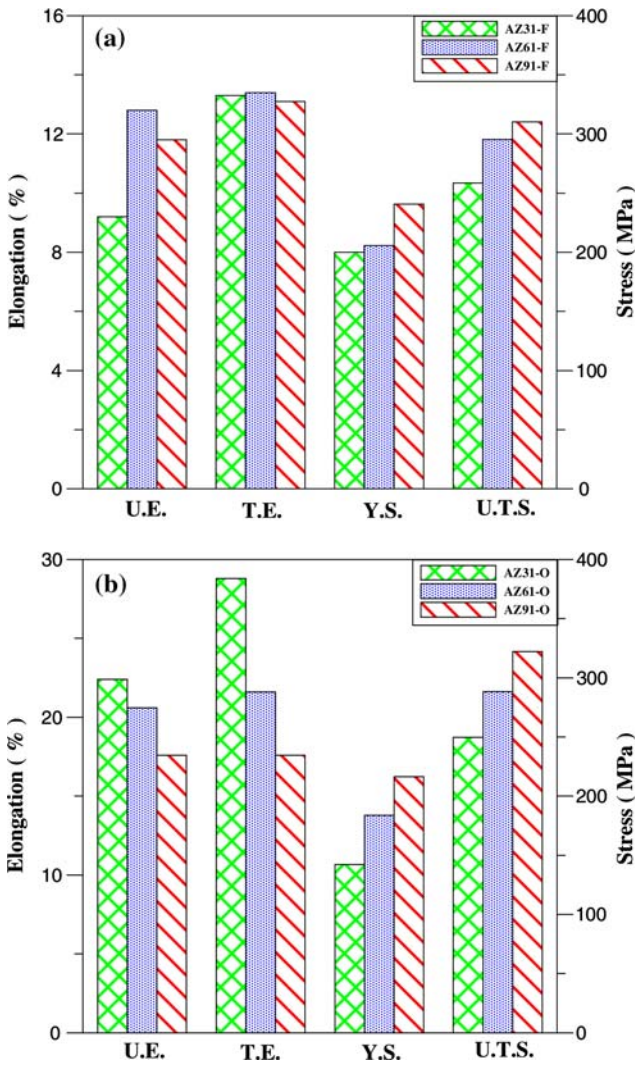

Fig. 11 Tensile mechanical properties: (**a**) the F specimens and (**b**) the O specimens

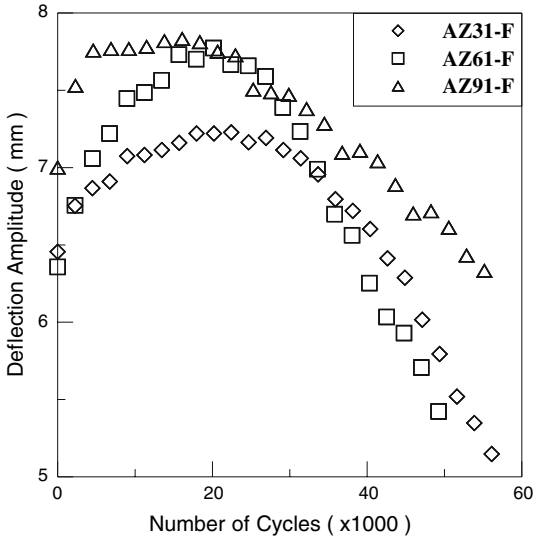

Fig. 12 *D–N* curves of the F specimens under a fixed vibration force of 1.3 G

Fig. 13a) and the twins form parallel to the vibration cracks, as seen in Fig. 13b. This result implies that the vibration twins formed during vibration deformation.

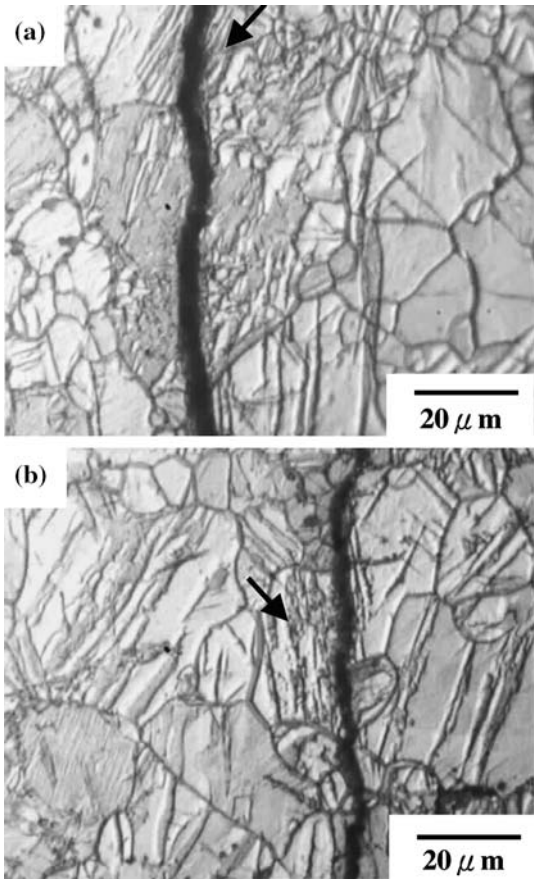

Fig. 13 Surface morphology of AZ31-F specimen after vibration-deformed: (**a**) vibration crack go through the twin and (**b**) the twin form and parallel to the vibration cracks

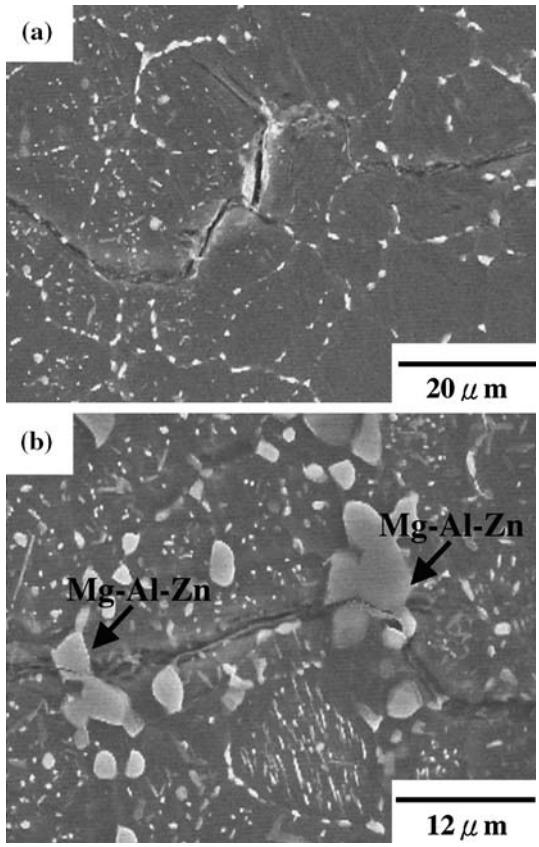

Fig. 14 Vibration deformed structures of AZ91-F specimen: (**a**) vibration twin and the intergranular fractures and (**b**) broken Mg–Al–Zn compounds alongside the main crack

However, the above-mentioned vibration twins can also be observed in the AZ91-F specimen and there are small cracks near the main crack (Fig. 14a). Intergranular fractures can also be seen in this image. Meanwhile, broken Mg–Al–Zn compounds alongside the main crack were observed under vibration testing (Fig. 14b). This explains how the Mg–Al–Zn compounds affect crack propagation during vibration.

Figure 15 shows the *D–N* curves of the O specimens under a fixed vibration force of 1.3 G. The results show that the vibration life of AZ91-O was highest, followed by AZ61-O and AZ31-O, respectively. The vibration life showed a reverse trend to that of the F specimens. From observation of vibration-deformed structures (AZ-O), we see that the number of both vibration twins and small vibration cracks increased with increasing Al content (see Fig. 16a, b). The twin effect can be separated into two parts: original twin and vibration twin. The original twin can deplete the vibration energy and lengthen the vibration life. This is the reason that the AZ31-F specimen possessed a longer vibration life than the other F specimens. In addition, the formation of a vibration twin can improve

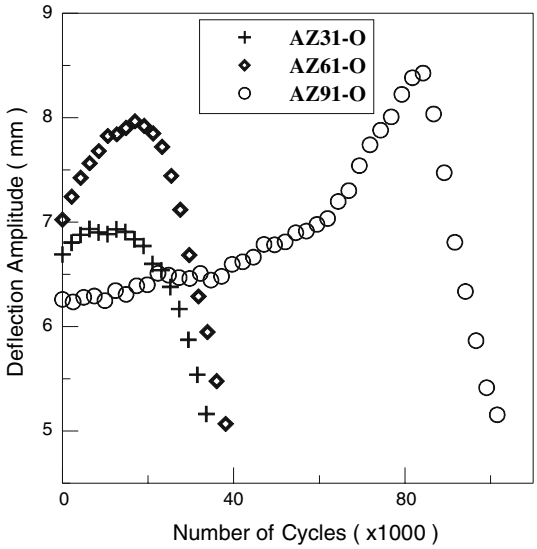

Fig. 15 *D–N* curves of the O specimens under a fixed vibration force of 1.3 G

the vibration life. After etching, vibration twins were also observed near the main crack (take AZ61-O for example, see Fig. 16c). Raising the Al content allows the vibration twins to form easily during vibration. So, the high Al fully annealed samples (AZ91-O) had greater vibration fracture resistance than the other O specimens. The effect of the proeutectic on the damping capacity is similar to the original twin and vibration twin, while the γ-$Mg_{17}Al_{12}$ in the grain boundary has no contribution to the vibration life and causes intergranular fractures to occur easily.

Vibration characteristics versus tensile deformation resistance

From Figs. 5 and 6, we see that the vibration life of the Al–Zn alloys increased with decreasing the Zn content. But the tensile strength of the Al–Zn alloys had an inverse tendency towards the vibration life. In another words, the vibration life of Al–*x*Zn alloys cannot be assessed from the tensile mechanical properties. Notably, similar results also occurred in the as-extruded AZ-F Mg alloys with various Al content (see Figs. 11, 13, and 15). As for the annealed AZ-O Mg alloys, the relationship between the vibration life and the tensile strength was roughly linear, while the number of vibration twins increased with increasing the vibration life.

For many engineering materials, the vibration fracture resistance increases with increasing the tensile deformation resistance of the materials [17, 18]. However, this is not true for all materials [2, 19–21]. The most likely explanation for this is that vibration testing not only involves fatigue, but also involves a vibration force with frequency of ~10^2 Hz unlike the tensile testing which has a strain rate of ~10^{-3} s^{-1}. Although the present two alloys had different structures, density, damping capacity and mechanical properties, the annealed AZ91-O not only contained lower specific weight, but also could form vibration twins during vibration, which lengthened the vibration life. For the above reasons, the light metals used for vibration must be chosen very carefully.

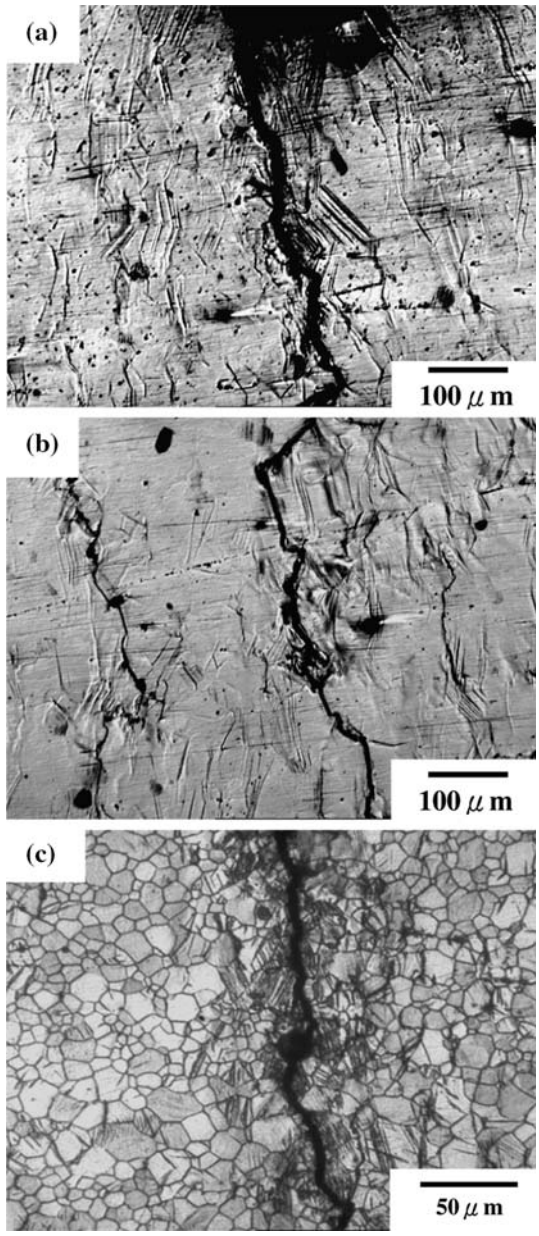

Fig. 16 Vibration deformed structures of AZ91-O specimens: (**a**) a greater quantity of twins and (**b**) a greater numbers of small cracks. (**c**) Vibration twins of AZ61-O specimens near the main crack

Conclusions

1. For quenched Al–Zn alloys, regardless of the vibration test conditions, low Zn specimens (7Zn) possessed a larger number of slip bands and fewer intergranular fracture areas. The results reveal that the 7Zn specimen had the highest crack propagation resistance and the longest vibration life.
2. Under constant force conditions, the vibration life of the as-extruded specimens in decreasing order was AZ31-F, AZ61-F, and then AZ91-F. However, the high Al fully annealed samples had greater vibration fracture resistance. Both original twins and vibration twins were able to lengthen the vibration life, while γ-$Mg_{17}Al_{12}$ offered no protection against vibration crack propagation.

Acknowledgements The authors are grateful to the Chinese National Science Council for its financial support (Contract: NSC 94-2216-E-006-008).

References

1. Moon BC, Lee ZH (1998) Scripta Mater 38(2):207
2. Masumoto H, Hinai M, Sawaya S (1983) Trans Jpn Inst Metals 24:681
3. Nuttall K (1971) J Inst Metals 99:266
4. Torisaka Y, Kojima S (1991) Acta Metall Mater 39(5):947
5. Polmear IJ (1996) Mater Trans JIM 37(1):12
6. Polmear IJ (1994) Mater Sci Technol 10(1):1
7. Zhang Z, Couture A, Luo A (1998) Scripta Mater 39(1):45
8. Tan JC, Tan MJ (2003) Mater Sci Eng A 339:124
9. Watanabe H, Mukai T, Kohzu M Tanabe S, Higashi K (1999) Acta Mater 47:3753
10. Kim WJ, Chung SW, Chung CS, Kum D (2001) Acta Mater 49:3337
11. Somehawa H, Hirai K, Watanabe H, Takigawa Y, Higashi K (2005) Mater Sci Eng A 407:53
12. Krishnamurthy S, Gupta SP (1977) Mater Sci Eng 30:167
13. Kovavs WJ, Low JR JR (1971) Metall Trans 2:3385
14. Kroggel R, Schierig H, Schiffmann R, Siebert P (1985) Crystal Res Technol 20(2):251
15. Zhu X (1990) J Appl Phys 67:7287
16. Clark JB (1968) Acta Metall 16:141
17. Horng JH, Lui TS, Chen LH (2001) Int J Cast Metals Res 14:121
18. Lin SC, Lui TS, Chen LH, Song JM (2002) Metall Mater Trans A 33A:2623
19. Hung FY, Lui TS (2005) J Mater Sci 40(14):3683
20. Song JM, Chang YL, Lui TS, Chen LH (2004) Mater Trans 45(3):666
21. Song YH, Lui TS, Chen LH (2004) Mater Trans 45(7):2463